

Thermal transport in graphyne nanoribbons

Tao Ouyang,^{1,*} Yuanping Chen,^{1,†} Li-Min Liu,² Yuee Xie,¹ Xiaolin Wei,¹ and Jianxin Zhong^{1,‡}

¹Laboratory for Quantum Engineering and Micro-Nano Energy Technology, Xiangtan University, Xiangtan 411105, Hunan, China

²Laboratory for Green Energy, Beijing Computational Science Research Center, Beijing 100084, China

(Received 28 February 2012; revised manuscript received 21 May 2012; published 19 June 2012)

Graphyne, a new allotrope of carbon, is a current topic of focus in the nanomaterial research community. We investigate the thermal transport property of graphyne nanoribbons (GYNRs) by using the nonequilibrium Green's-function method. The thermal conductance of GYNRs is only approximately 40% that of graphene nanoribbons. A distinct width dependence of the thermal property is observed in GYNRs as well. The conductance of armchair-edged GYNRs (A-GYNRs) shows a linear width dependence, while a steplike width dependence is displayed in the conductance of zigzag-edged GYNRs (Z-GYNRs). Moreover, the conductance of an A-GYNR is larger than that of a Z-GYNR of the same width, indicating obvious anisotropic transport in graphyne (twice that in graphene). In addition, the thermal transport in graphyne family nanoribbons is also explored. The results show that the conductance of graphyne family nanoribbons is insensitive to the acetylenic linkages, but depends on the number of benzene rings. These findings could offer useful guidelines for the design and performance improvement of the graphyne-based nanodevices.

DOI: [10.1103/PhysRevB.85.235436](https://doi.org/10.1103/PhysRevB.85.235436)

PACS number(s): 65.80.Ck, 63.22.Np, 81.07.-b, 81.05.U-

I. INTRODUCTION

Recently, the thermal properties of graphene and its derivatives have attracted considerable attention due to the great potential applications.^{1,2} Many fascinating thermal behaviors and phenomena have been gradually revealed in this low-dimensional carbon nanomaterial.²⁻¹³ For instance, the room-temperature thermal conductivity of suspended graphene is as high as ~ 5000 W/mK and it can be modulated by the quantity of the atomic layers.³⁻⁵ Obvious anisotropic thermal transport is also reported in graphene nanoribbons (GNRs) with different edge chirality.^{7,8} More interestingly, the asymmetric graphene nanostructures are found to have exceptional thermal rectification efficiency.¹⁰⁻¹² These impressive thermal properties mainly originate from its novel structural characteristics, which are the basis for a complete understanding of thermal transport in graphene.

Graphyne, another layered carbon allotrope containing both sp and sp^2 hybridized carbon atoms,¹⁴ is a new topic in the current nanomaterial research community. Consisting of the same element, graphyne has some eximious properties analogous to graphene, such as high carrier mobility,¹⁵ strong mechanical properties,¹⁶ and excellent chemical and thermal stability.¹⁷ However, its peculiar structural characteristic (the existence of acetylenic linkage) also introduces a rich variety of physical properties¹⁸⁻²³ that are quite different from those in graphene. For example, graphyne is a narrow gap semiconductor and its band gap can be modified continuously under strain.¹⁸⁻²⁰ Exceptional optical properties are predicted as well in this new two-dimensional carbon nanostructure,^{15,18,21} including high third-order nonlinear optical susceptibility, strongly anisotropic optical adsorption, and high fluorescence efficiency. These intriguing properties¹⁵⁻²³ and recent experimental progress²⁴ foreshow the technology applications of graphyne ranging from optoelectronic devices to energy storage, making it one of the hottest topics in carbon-based materials. Nevertheless, previous studies focused mainly on its electronic, optical, and mechanical properties. The effect of acetylenic

linkage on the thermal transport property of graphyne, especially its basic building blocks of applications—graphyne nanoribbons (GYNRs)—has not received significant attention until now. Therefore, in order to ensure successful application, it is desirable to explore how the peculiar structural characteristics impact thermal transport in graphyne and GYNRs.

In this paper we investigate the effects of structural characteristics, e.g., edge chirality and geometric size, on the thermal conductance of GYNRs. The results show that the existence of acetylenic linkage indeed leads to different thermal transport properties between graphyne and graphene. The thermal conductance of GYNRs is approximately 40% that of GNRs, which is suggestive of potential thermoelectric applications. Compared to the linear width dependence of thermal conductance in GNRs, distinct thermal behaviors are observed in GYNRs with different edge chirality. For armchair-edged GYNRs (A-GYNRs), the conductance presents a linear width dependence, while a steplike width dependence is displayed in zigzag-edged GYNRs (Z-GYNRs). Meanwhile, the A-GYNR is shown to have a larger thermal conductance than that of the Z-GYNR, implying obvious anisotropic thermal transport in graphyne (twice that in graphene). Through an analysis of the phonon spectra and boundary condition of GYNRs, we illustrate the origin of this anisotropic property. In addition, thermal transport in GYNRs with different numbers of acetylenic linkage (referred to as graphyne family nanoribbons) is also explored. It is found that the conductance in the graphyne family is insensitive to the acetylenic linkages but is closely associated with the number of benzene rings. These findings could provide useful guidelines for the applications of graphyne not only in nanodevices, but also in thermal management.

II. MODEL AND METHOD

By cutting an infinite graphyne sheet along different directions, we can obtain two typical edged GYNRs: A-GYNRs [see Fig. 1(a)] and Z-GYNRs [see Fig. 1(b)]. The

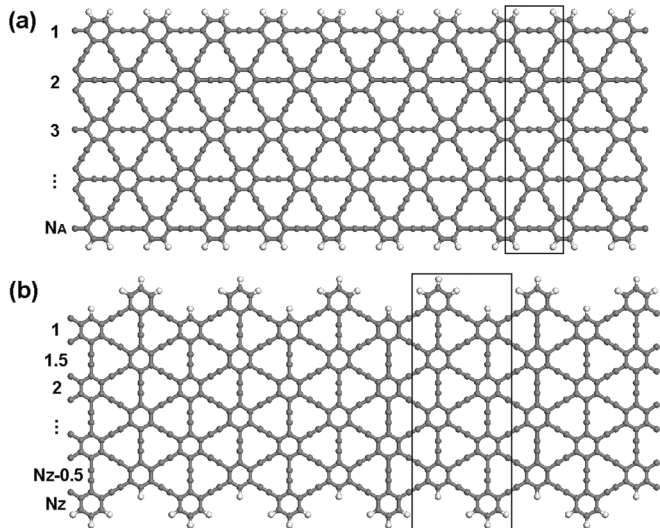


FIG. 1. The A-GYNRs and Z-GYNRs can be obtained by cutting through an infinite graphyne sheet along two different directions: (a) A-GYNRs with a width of N_A and (b) Z-GYNRs with a width of N_Z . Unlike in the A-GYNRs, the width of Z-GYNRs can differ by a half integer. The black pane denotes their corresponding unit cell.

width of A-GYNRs (Z-GYNRs) is denoted by N_A (N_Z), which is determined by the number of benzene rings. Unlike the width definition of A-GYNRs, in the Z-GYNRs the width definition can possess a half integer due to the unique structure of graphyne. Similarly, graphdiyne and the graphyne-family nanoribbons can be easily obtained from GYNRs merely by replacing one acetylenic linkage with two or more acetylenic linkages between two nearest-neighbor benzene rings. For convenience of illustration, the number of acetylenic linkages is employed to distinguish the graphdiyne and graphyne-family nanoribbons. For example, A-GYNR- n and Z-GYNR- n ($n \geq 2$) denote the armchair-edged and zigzag-edged graphyne nanoribbons, respectively, with n -acetylenic linkages between two nearest-neighbor benzene rings. To avoid edge reconstruction, the edge carbon atoms of GYNRs are H passivated. Since recent theoretical and experimental studies show that graphyne

is semiconducting,^{18–20} the thermal transport contributed by phonons is considered only in our calculations.

The second-generation Brenner bond-order potential,²⁵ which gives an excellent description of carbon-carbon bonding interactions, is employed to optimize the geometric structure. The optimized structure of graphyne based on this empirical potential is presented in Fig. 2(a); it is in good agreement with the first-principles calculations, in particular the carbon bonds around benzene ring [see Fig. 2(b)].²⁶ From the fully relaxed structure the phonon spectra of graphyne calculated from the Brenner potential and the density-function theory²⁶ (DFT) are presented in Figs. 2(c) and 2(d), respectively. One can see that the low-frequency phonon modes ($<1000 \text{ cm}^{-1}$) calculated from this empirical potential are in excellent agreement with the results based on the DFT, while the high-frequency phonons do not coincide with the DFT data in detail. However, we can safely ignore the effect of these high-frequency phonon modes on the phonon thermal transport due to their very low phonon group velocities. Moreover, the contribution of these high-frequency phonons to the thermal conductance is generally negligible. Therefore, the Brenner bond-order potentials can describe the phonon thermal conductance of graphyne-based nanostructures reasonably well.

Based on the fully relaxed structure, the force constants for each atom are obtained from the equilibrium position under small displacements. Then the thermal transport properties can be calculated by using the nonequilibrium Green's-function (NEGF) method.^{27–29} According to the NEGF scheme, the retarded Green's function G^r of this nanostructure is expressed as

$$G^r = \left[(\omega + i0^+)^2 I - K^C - \sum_L^r - \sum_R^r \right]^{-1}, \quad (1)$$

where ω is the frequency of the phonons, I is an identity matrix, and K^C is the mass-weighted force constant matrix of the central region. The term $\sum_\beta^r = V^{C\beta} g_\beta^r V^{\beta C}$ ($\beta = L, R$, corresponding to the left and right thermal leads, respectively) denotes the self-energy of the thermal lead β , in which $V^{\beta C} = (V^{C\beta})^T$ is the coupling matrix of the lead β to the central region and g_β^r is the lead surface Green's function. Here g_β^r

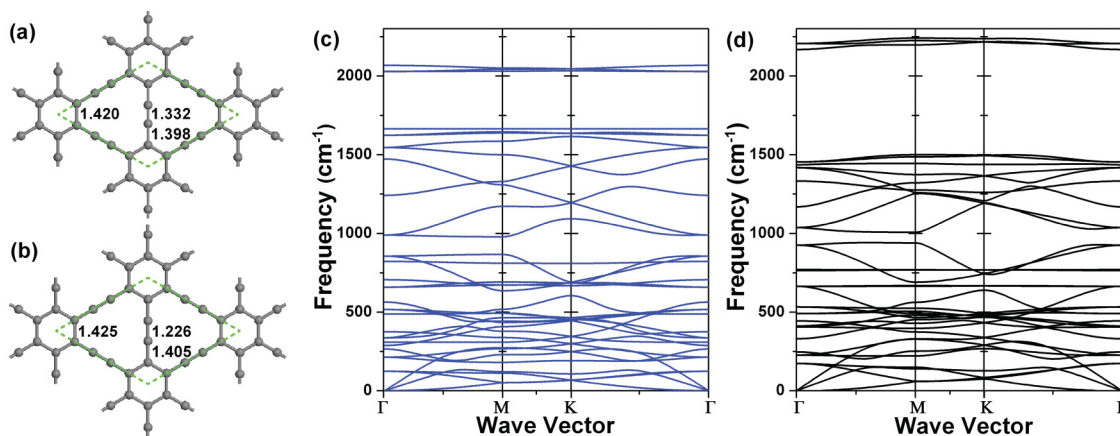


FIG. 2. (Color online) Optimized structure of graphyne based on (a) the Brenner bond-order potential and (b) the density-functional theory (DFT), where the unit of bond length is angstroms. The green pane denotes the unit cell of graphyne. The phonon spectra of graphyne calculated from (c) the Brenner bond-order potential and (d) the DFT. Details of the calculations for the DFT are presented in Ref. 26.

is calculated by $g_\beta^r = [(\omega + i0^+)^2 I - K_{00}^\beta - K_{01}^\beta \Lambda]^{-1}$, where K_{00}^β and K_{01}^β are the force constant and coupling matrices, respectively, for a unit cell in thermal lead β , and Λ is the appropriate transfer matrix, which can be calculated from the force constant matrix element via an iterative procedure.²⁹ Once the retarded Green's function G^r is obtained, we can calculate the transmission coefficient $T[\omega]$ and then the thermal conductance σ of nanoribbons:²⁹

$$T[\omega] = \text{Tr}\{G^r \Gamma_L G^a \Gamma_R\}, \quad (2)$$

$$\sigma(T) = \frac{\hbar}{2\pi} \int_0^\infty T[\omega] \omega \frac{\partial f(\omega)}{\partial T} d\omega, \quad (3)$$

where $\Gamma_\beta = i(\sum_\beta^r - \sum_\beta^a) = -2\text{Im}V^{C\beta} g_\beta^r V^{\beta C}$ is the coupling function of the β lead and $f(\omega) = [\exp(\hbar\omega/k_B T) - 1]^{-1}$ is the Bose-Einstein distribution function for a heat carrier at the leads. Meanwhile, the phonon local density of states on the i th atom of the central scattering region can also be given by the NEGF $\rho_i(\omega) = i\omega(G_{ii}^r - G_{ii}^a)/\pi$.

In addition, the phonon spectrum of the GYNR can be obtained from the generalized eigenvalue method:²⁹

$$\begin{pmatrix} \omega^2 I - K_{11} & I \\ K_{10} & 0 \end{pmatrix} \begin{pmatrix} \varepsilon \\ \zeta \end{pmatrix} = \lambda \begin{pmatrix} K_{01} & 0 \\ 0 & I \end{pmatrix} \begin{pmatrix} \varepsilon \\ \zeta \end{pmatrix}. \quad (4)$$

After diagonalizing this generalized eigenvalue matrix, one can get the eigenvalues λ . The wave number q for a special ω

is found by selecting the traveling-wave eigenvalue ($\lambda = e^{iqa}$). Then the phonon spectrum of the nanoribbons is obtained.

III. RESULTS AND DISCUSSION

In Figs. 3(a) and 3(b) we depict the thermal conductance as a function of temperature for A-GYNRs and Z-GYNRs, respectively, with different widths. Because the phonon modes are gradually excited as temperature increases, the thermal conductance of all GYNRs increases with temperature. Meanwhile, one can find that the conductance displays a different temperature dependence on the width of GYNRs. In the narrow GYNRs [$N_A(N_Z) = 1$] the numbers of phonon modes is quite limited and thus the thermal conductance varies slowly with increasing temperature. In the wider GYNRs, however, more phonon modes can be generated, which will provide a greater contribution to the thermal transport. As a result, the thermal conductance increases rapidly with temperature. Furthermore, by comparing Figs. 3(a) and 3(b) one can see that the two edged GYNRs possess a different width dependence. To show this discrepancy more clearly, the thermal conductance of A-GYNRs and Z-GYNRs versus the width is described in Figs. 3(c) and 3(d). For A-GYNRs the thermal conductance varies linearly as the width increases and the slope of the curves increases as temperature increases. This linear width dependence of thermal conductance is

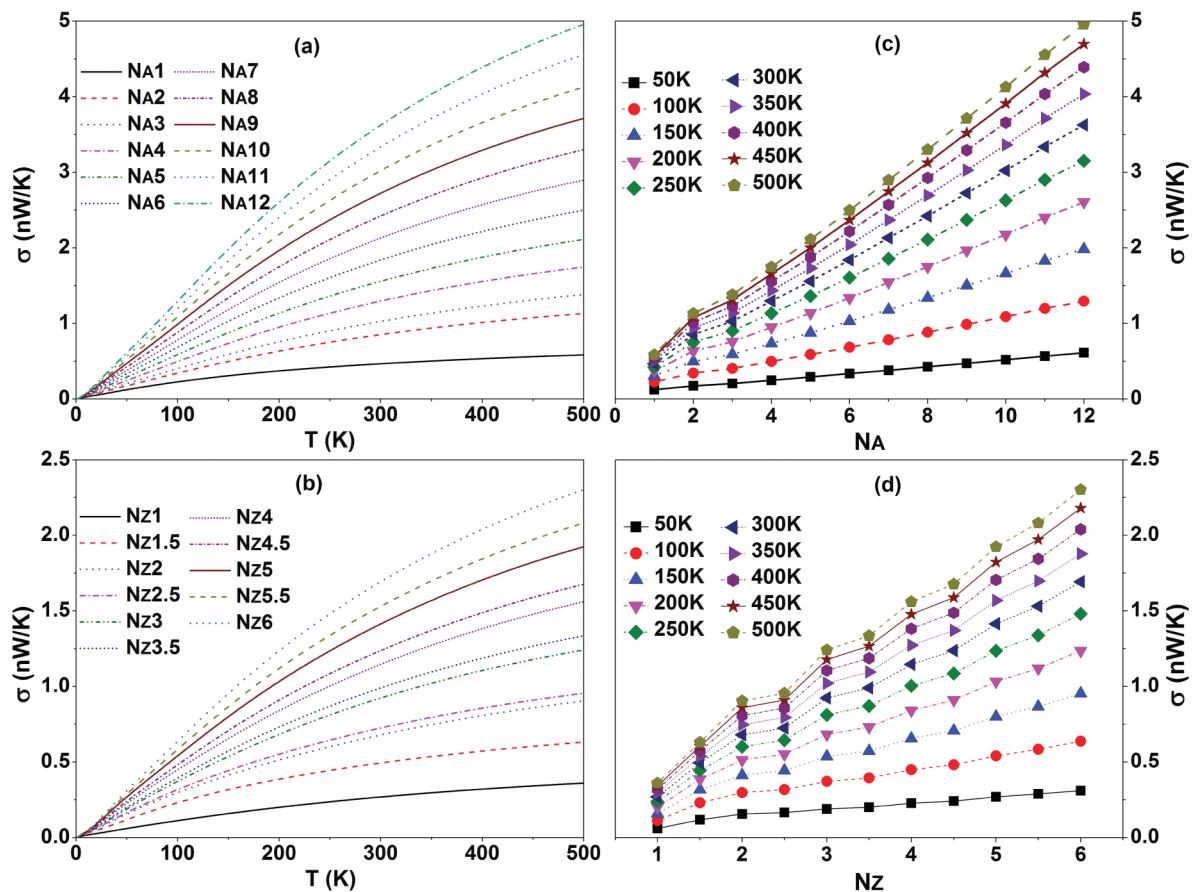


FIG. 3. (Color online) Thermal conductance of (a) A-GYNRs and (b) Z-GYNRs as a function of temperature T at different widths and (c) A-GYNRs and (d) Z-GYNRs as a function of width at different temperatures.

because in the ballistic thermal transport region the number of phonon modes depends linearly on the width of A-GYNRs. Similar thermal phenomena have also been reported in other honeycomb lattice nanoribbons, e.g., graphene nanoribbons³⁰ and boron-nitride nanoribbons³¹ (BNNRs). Nevertheless, one can find from Fig. 3(d) that the thermal conductance of Z-GYNRs presents steplike width dependence, especially when the width is narrower than $N_Z = 4.5$. This unique thermal behavior is mainly attributed to the peculiar structural characteristics of graphyne. When the width of Z-GYNRs increases from an integer to a half integer, the increasing width can result in more phonon modes, but the narrow part of the nanoribbons dominates the thermal transport and will restrict the quantity of traveling phonon modes (phonon transport channels). Therefore, the phonon modes derived from the increasing width cannot contribute to the thermal transport efficiently, which gives rise to the steplike width dependence of thermal conductance in Z-GYNRs. As the width of Z-GYNRs increases further, the restrictive effect from the narrow part becomes weak and thus the steplike behavior gradually disappears and the linear dependence reappears in the thermal conductance.

To directly compare the difference of thermal transport properties between the two edged GYNRs, the scaled thermal conductance σ/S as a function of the practical width W for both A-GYNRs and Z-GYNRs at room temperature (300 K) is depicted in Fig. 4. Herein the cross sectional area S is defined as $S = Wh$, where $h = 0.345$ nm is chosen as the layer separation of bulk graphyne.³² One can find from Fig. 4 that the effects of both edge shape and practical width play significant roles in the scaled thermal conductance of GYNRs. For the A-GYNR cases, the scaled thermal conductance for the narrower nanoribbons (< 3 nm) decreases rapidly as the practical width increases and changes quite slowly for wider nanoribbons. For GYNRs with a zigzag edge, however, there exists an oscillatory behavior in the scaled thermal

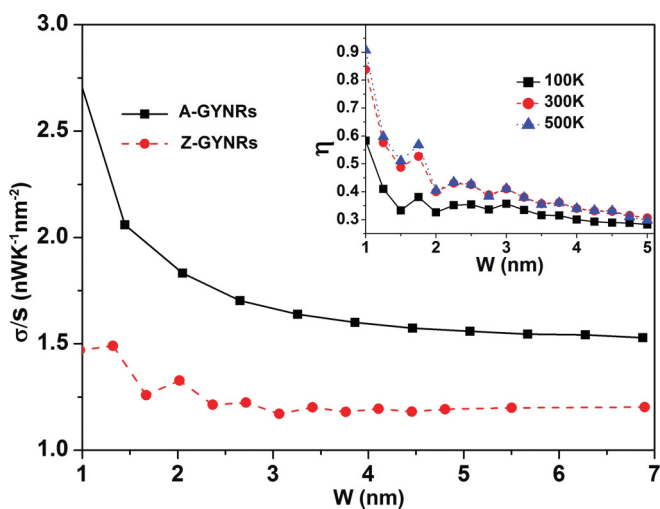


FIG. 4. (Color online) Scaled thermal conductance σ/S as a function of practical width W for A-GYNRs and Z-GYNRs at room temperature (300 K). The inset shows the anisotropy factor η as a function of practical width W for graphyne nanoribbons at three typical temperatures.

conductance especially when the practical width is narrower than 3 nm. This is mainly attributed to the steplike width dependence of thermal conductance. With the large practical width limited, the scaled thermal conductance of GYNRs reaches different stable values, which are approximately 1.52 and 1.2 nW/K/nm^2 for A-GYNRs and Z-GYNRs, respectively. The stable scaled thermal conductance in GYNRs is approximately 40% of that in GNRs (approximately 3.6–4.2 nW/K/nm^2),⁷ implying that the thermal transport property of graphyne is quite weaker than that of graphene. Meanwhile, the obvious different scaled thermal conductance between these two edged GYNRs also reveals the anisotropic thermal transport property in graphyne. It is worth noting that the anisotropic thermal property in graphyne is opposite that in graphene, where GNRs with a zigzag edge are higher than the nanoribbons with an armchair edge. To give a quantitative description of the anisotropic thermal conductance, the anisotropy factor η ($\eta = [(\sigma/S)_{\text{A-GYNR}}/(\sigma/S)_{\text{Z-GYNR}} - 1]$) of GYNRs is plotted in the inset of Fig. 4. It can be seen that the narrow GYNRs generally possess a large thermal anisotropy, although the anisotropy factor is irregular in this region (< 3 nm). When the practical width increases further, the anisotropy factor decreases slowly and gradually tends to a stable value. Moreover, one can find that the anisotropy factor of GYNRs is insensitive to temperature, especially for the wider nanoribbons. Analogous thermal anisotropy phenomena have also been observed in GNRs⁷ and BNNRs.³¹ Compared to these nanomaterials, the graphyne possesses stronger anisotropic thermal transport properties. For example, when the practical width is 5 nm the anisotropy factor of graphyne is approximately 30% at room temperature (300 K), while it is only 16% and 20% for graphene⁷ and hexagonal boron nitride³¹ for the same condition. This indicates that the anisotropic thermal transport property of graphyne could be measured more evidently in experiment than that of graphene.

In Fig. 5 the phonon spectra and phonon transmission coefficient for A-GYNR with $N_A = 4$ (approximately 2.0498 nm) and Z-GYNR with $N_Z = 3$ (approximately 2.0286 nm) are depicted to elucidate the anisotropic thermal transport property. Comparing Figs. 5(a) and 5(b), one can find that the phonon bands (phonon modes) in A-GYNR have a larger slope (group velocity) than that in Z-GYNR, where there are many flat bands. That is, the phonon spectrum in A-GYNRs is more dispersive than that in Z-GYNRs. This discrepancy mainly originates from the unique geometric structure of Z-GYNR, which can generate more localized lattice vibrations than the nanoribbons with an armchair edge. Just because of this more dispersive phonon spectrum, there are more phonon bands at a given frequency for the A-GYNRs. In the ballistic transport region the phonon transmission coefficient $T[\omega]$ essentially equals the number of phonon bands at a frequency ω .^{29,33} As a result, one can see from Fig. 5(c) that the A-GYNR possesses a larger phonon transmission than the Z-GYNR, especially in the frequency range from 0 to 1000 cm^{-1} . Consequently, a higher thermal conductance exists in A-GYNRs, thus leading to the anisotropic thermal transport property in graphyne. Besides the intrinsic structural characteristic, the boundary condition is also an important factor in the thermal anisotropy of graphyne. In Fig. 6 we describe the scaled thermal conductance σ/S for the A-GYNR with $N_A = 4$ and the Z-GYNR with $N_Z = 3$ at

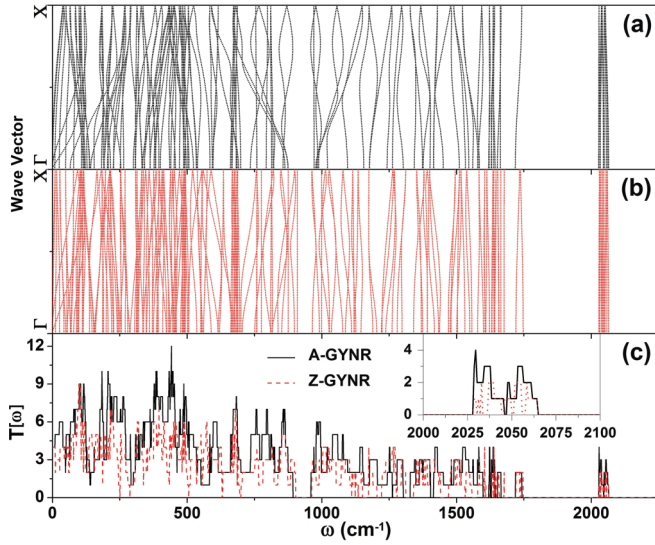


FIG. 5. (Color online) Phonon spectra for (a) A-GYNR with $N_A = 4$ and (b) Z-GYNR with $N_Z = 3$. (c) Corresponding phonon transmission coefficient $T[\omega]$ (solid and dotted lines are for A-GYNR and Z-GYNR, respectively). The inset of (c) is the phonon transmission coefficient in the extremely-high-frequency region (2000–2100 cm^{-1}).

free and fixed boundary conditions (by setting the edge atoms to 1×10^7 amu).⁷ One can find that the fixed edge atoms lead to a decrease in σ/S for both GYNRs. The σ/S of the A-GYNR decreases markedly, especially at high temperatures, whereas the decrease in the Z-GYNR is relatively small (see the inset of Fig. 6). After imposing fixed boundary conditions, the thermal anisotropy becomes smaller (before $\eta = 38.2\%$ and after $\eta = 19.8\%$), but does not disappear. This indicates that the effect of boundary conditions plays a more important role in A-GYNRs than in Z-GYNRs. Therefore, in the case

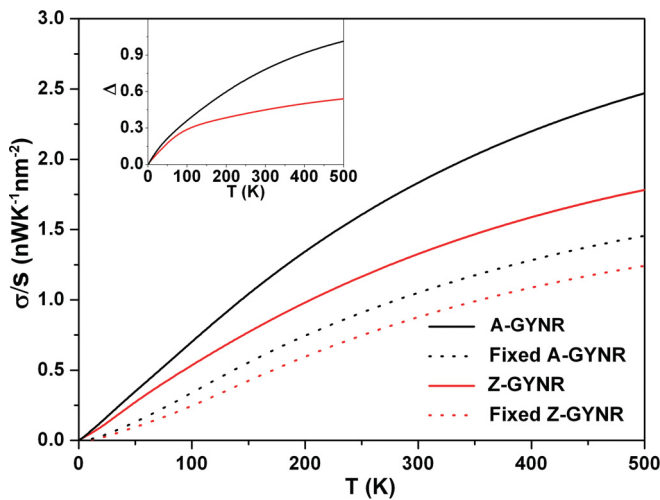


FIG. 6. (Color online) Scaled thermal conductance σ/S vs temperature T for A-GYNR with $N_A = 4$ (black line) and Z-GYNR with $N_Z = 3$ (red line), where the solid and dotted lines represent the nanoribbons with free and fixed boundary conditions, respectively. The inset shows the decrease in scaled thermal conductance Δ [$\Delta = (\sigma/S)_{\text{free}} - (\sigma/S)_{\text{fixed}}$] induced by fixing edge atoms.

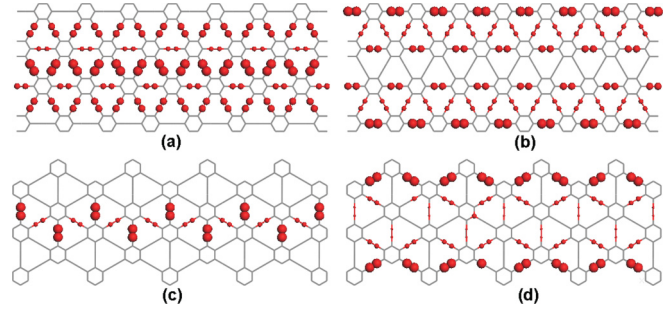


FIG. 7. (Color online) (a) and (b) Phonon local density of states for the A-GYNR at two typical frequencies of 2030 and 2048 cm^{-1} . (c) and (d) Local density of states for the Z-GYNR at two typical frequencies of 2029 and 2043 cm^{-1} .

of free boundary conditions the thermal conductance is higher for A-GYNRs than for Z-GYNRs.

In addition, one can find from Figs. 5(a) and 5(b) that there exists a phonon mode group in the high-frequency regime (2025–2075 cm^{-1}) for both A-GYNRs and Z-GYNRs. Although there are numerous phonon modes, their slope is quite small and thus the corresponding phonon transmission coefficient is small as well [see the inset of Fig. 5(c)]. In order to illustrate the origin of these phonon modes, the phonon local density of states at some typical frequencies are plotted in Fig. 7. It can be seen clearly that all these phonon states for both A-GYNRs and Z-GYNRs are intensively localized around the acetylenic linkages, i.e., the phonon modes are mainly derived from the vibrational states of the carbon atoms in acetylenic linkages. Since the bonding length of these carbon atoms is smaller and its corresponding bonding energy is stronger than that in the benzene ring [see Fig. 2(a)], the phonon modes are mainly distributed in the high-frequency region. The contribution from these high-frequency phonon modes to the thermal transport is quite small according to the weight factor $\omega df(\omega)/dT$ in Eq. (3). Therefore, one can

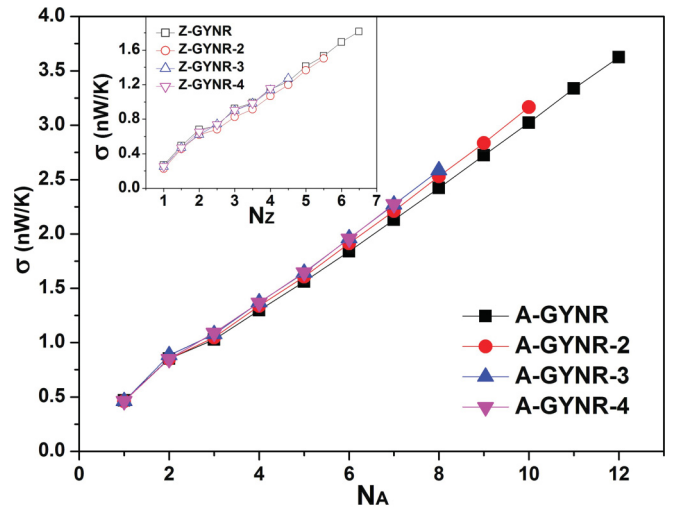


FIG. 8. (Color online) Thermal conductance as a function of width for the armchair-edged graphyne-family nanoribbons (A-GYNR- n , $n \geq 2$). The inset shows the thermal conductance for the zigzag-edged graphyne-family nanoribbons (Z-GYNR- n , $n \geq 2$).

expect that the increase of acetylenic linkage will not bring obvious changes to the thermal conductance of graphyne.

In Fig. 8 the thermal conductance as a function of width (number of benzene rings) for the graphyne nanoribbons with different numbers of acetylenic linkage (referred to as graphyne-family nanoribbons) is depicted to demonstrate the above conjecture. As expected, one can find that although the geometric structure changes a lot, the ballistic thermal conductance of the GYNR- n with both an armchair edge and a zigzag edge (see the inset of Fig. 8) changes only slightly in the whole width range studied here. So we can conclude that the thermal conductance of graphyne-family nanoribbons is insensitive to the numbers of acetylenic linkage but depends on the numbers of benzene rings. That is, at the same practical width, the graphyne-family nanoribbons with more acetylenic linkages will possess a lower thermal conductance, thereby suggesting potential thermoelectric applications. In addition, this result also indicates that if one can measure the thermal conductance in any type of graphyne nanoribbon, the thermal properties of other graphyne-family nanoribbons could be evaluated approximately.

IV. CONCLUSION

In conclusion, the thermal transport properties of graphyne were systematically investigated by using the NEGF method. The effects of both edge shape and width on the thermal conductance of GYNRs were discussed. The results show that

the existence of acetylenic linkage indeed leads to different thermal transport properties between graphyne and graphene. The thermal conductance of GYNRs is approximately 40% that of GNRs, which is suggestive of the potential thermoelectric applications. Moreover, it was found that the conductance in A-GYNRs presents a linear width dependence, while it displays a steplike width dependence for Z-GYNRs. Compared with graphene, a stronger anisotropic thermal transport property is observed in graphyne that is approximately two times larger than that in graphene. The origin of this anisotropic thermal transport property is illustrated by analyzing the phonon spectra and boundary conditions of two edged GYNRs. As the phonon modes derived from the acetylenic linkages are mainly distributed at high frequency, the thermal conductance of the graphyne family is insensitive to the number of acetylenic linkages but depends on the number of benzene rings. These results may provide useful guidelines for the application of graphyne not only in nanodevices but also in thermal management.

ACKNOWLEDGMENTS

This work was supported by the National Basic Research Program of China (Grant No. 2012CB921300), the National Natural Science Foundation of China (Grants No. 11074211, No. 51172191, No. 51006086, No. 11074213, and No. 51176161), and Joint Funds of the Hunan Provincial Natural Science Foundation of China (Grant No. 10JJ9001).

*ouyangtao@xtu.edu.cn

†chenyp@xtu.edu.cn

‡jxzhong@xtu.edu.cn

¹A. H. Castro Neto, F. Guinea, N. M. R. Peres, K. S. Novoselov, and A. K. Geim, *Rev. Mod. Phys.* **81**, 109 (2009).

²A. A. Balandin, *Nature Mater.* **10**, 569 (2011).

³A. A. Balandin, S. Ghosh, W. Bao, I. Calizo, D. Teweldebrhan, F. Miao, and C. N. Lau, *Nano Lett.* **8**, 902 (2008).

⁴D. L. Nika, S. Ghosh, E. P. Pokatilov, and A. A. Balandin, *Appl. Phys. Lett.* **94**, 203103 (2009).

⁵S. Ghosh, W. Bao, D. L. Nika, S. Subrina, E. P. Pokatilov, C. N. Lau, and A. A. Balandin, *Nature Mater.* **9**, 555 (2010).

⁶T. Ouyang, Y. P. Chen, Y. E. Xie, G. M. Stocks, and J. X. Zhong, *Appl. Phys. Lett.* **99**, 233101 (2011).

⁷Y. Xu, X. B. Chen, B. L. Gu, and W. H. Duan, *Appl. Phys. Lett.* **95**, 233116 (2009).

⁸J. W. Jiang, J. S. Wang, and B. Li, *Phys. Rev. B* **79**, 205418 (2009).

⁹J. N. Hu, Y. Wang, A. Vallabhaneni, X. L. Ruan, and Y. P. Chen, *Appl. Phys. Lett.* **99**, 113101 (2011).

¹⁰J. N. Hu, X. L. Ruan, and Y. P. Chen, *Nano Lett.* **9**, 2730 (2009).

¹¹N. Yang, G. Zhang, and B. W. Li, *Appl. Phys. Lett.* **95**, 033107 (2009).

¹²T. Ouyang, Y. P. Chen, Y. Xie, X. L. Wei, K. K. Yang, P. Yang, and J. X. Zhong, *Phys. Rev. B* **82**, 245403 (2010).

¹³Y. Xu, X. B. Chen, J. S. Wang, B. L. Gu, and W. H. Duan, *Phys. Rev. B* **81**, 195425 (2010).

¹⁴R. H. Baughman, H. Eckhardt, and M. Kertesz, *J. Chem. Phys.* **87**, 6687 (1987).

¹⁵M. Q. Long, L. Tang, D. Wang, Y. L. Li, and Z. G. Shuai, *ACS Nano* **5**, 2593 (2011).

¹⁶S. W. Cranford and M. J. Buehler, *Carbon* **49**, 4111 (2011).

¹⁷N. Narita, S. Nagai, S. Suzuki, and K. Nakao, *Phys. Rev. B* **58**, 11009 (1998).

¹⁸J. Kang, J. B. Li, F. M. Wu, S. S. Li, and J. B. Xia, *J. Phys. Chem. C* **115**, 20466 (2011).

¹⁹J. Zhou, K. Lv, Q. Wang, X. S. Chen, Q. Sun, and P. Jena, *J. Chem. Phys.* **134**, 174701 (2011).

²⁰L. D. Pan, L. Z. Zhang, B. Q. Song, S. X. Du, and H. J. Gao, *Appl. Phys. Lett.* **98**, 173102 (2011).

²¹G. Luo, X. Qian, H. Liu, R. Qin, J. Zhou, L. Li, Z. Gao, E. Wang, W. N. Mei, J. Lu, Y. Li, and S. Nagase, *Phys. Rev. B* **84**, 075439 (2011).

²²H. Y. Zhang, M. W. Zhao, X. J. He, Z. H. Wang, X. J. Zhang, and X. D. Liu, *J. Phys. Chem. C* **115**, 8845 (2011).

²³C. Li, J. B. Li, F. M. Wu, S. S. Li, J. B. Xia, and L. W. Wang, *J. Phys. Chem. C* **115**, 23221 (2011).

²⁴G. X. Li, Y. L. Li, H. B. Liu, Y. B. Guo, Y. J. Li, and D. B. Zhu, *Chem. Commun.* **46**, 3256 (2010).

²⁵D. W. Brenner, O. A. Shenderova, J. A. Harrison, S. J. Stuart, B. Ni, and S. B. Sinnott, *J. Phys.: Condens. Matter* **14**, 783 (2002).

²⁶The structures are optimized by using the plane-wave basis projector-augmented wave method (Ref. 34) in the framework of density-functional theory within the generalized gradient approximation as implemented in the VASP code (Ref. 35). The plane-wave energy cutoff is set at 400 eV and the Perdew-Burke-Ernzerhof functional is used. Atoms are relaxed until the residual force is less

than $0.001 \text{ eV}/\text{\AA}$ and the total energies converge to $1 \times 10^{-5} \text{ eV}$. To avoid the interaction between adjacent images, a 15-\AA vacuum perpendicular to the graphyne sheet is employed. The Brillouin zone integration is carried out with a $(13 \times 13 \times 1)$ k mesh. Lattice dynamics are simulated with the PHONOPY code and the forces are calculated via VASP. In order to get an accurate phonon frequency, a $3 \times 3 \times 1$ supercell is used with an energy convergence of $1 \times 10^{-8} \text{ eV}$ and an energy cutoff of 500 eV .

²⁷N. Mingo, *Phys. Rev. B* **74**, 125402 (2006).

²⁸T. Yamamoto and K. Watanabe, *Phys. Rev. Lett.* **96**, 255503 (2006).

²⁹J. S. Wang, J. Wang, and J. T. Lu, *Eur. Phys. J. B* **62**, 381 (2008).

³⁰J. H. Lan, J. S. Wang, C. K. Gan, and S. K. Chin, *Phys. Rev. B* **79**, 115401 (2009).

³¹T. Ouyang, Y. P. Chen, Y. E. Xie, K. K. Yang, Z. G. Bao, and Jianxin Zhong, *Nanotechnology* **21**, 245701 (2010).

³²N. Narita, S. Nagai, S. Suzuki, and K. Nakao, *Phys. Rev. B* **62**, 11146 (2000).

³³Z. W. Tan, J. S. Wang, and C. K. Gan, *Nano Lett.* **11**, 214 (2011).

³⁴P. E. Blochl, *Phys. Rev. B* **50**, 17953 (1994); G. Kresse and D. Joubert, *ibid.* **59**, 1758 (1999).

³⁵G. Kresse and J. Furthmuller, *Phys. Rev. B* **54**, 11169 (1996); *Comput. Mater. Sci.* **6**, 15 (1996).